Nanoscale Advances

ROYAL SOCIETY OF CHEMISTRY

PAPER

View Article Online
View Journal | View Issue

Cite this: *Nanoscale Adv.*, 2024, **6**, 4858

Advanced lightweight lightning strike protection composites based on super-aligned carbon nanotube films and thermal-resistant zirconia fibers†

Mingquan Zhu,‡[ab] Peng Zhang,‡[ad] Feng Gao,‡[a] Yunxiang Bai,*[ab] Hui Zhang,*[a] Min Zu,[e] Luqi Liu[ab] and Zhong Zhang*[ac]

Received 10th May 2024
Accepted 20th July 2024

DOI: 10.1039/d4na00392f

rsc.li/nanoscale-advances

Carbon nanotube films have drawn attention in the past decade as promising substitutes for aluminum or copper used in aircraft lightning strike protection (LSP) systems. Throughout this study, advanced lightweight lightning strike protection (LSP) composites are based on highly conductive super-aligned carbon nanotube films (SA-CNTFs) and a new isolation layer of zirconia fiber paper. The internal damage level of the composite laminate was assessed using a microfocus X-ray system and non-destructive ultrasonic techniques. Results show that the composite laminate comprising SA-CNTFs (1000-layer) and zirconia fiber paper (1-layer) effectively shields CFRP from 100 kA lightning strikes. Furthermore, weight reductions of approximately 44.3% and 10.4% can be achieved, respectively, relative to the isolation layer of glass fibers and quartz fibers. Meanwhile, the lightning protection mechanism was further studied.

Introduction

Non-metallic composites like carbon fiber (CFRP) and glass fiber-reinforced polymers (GFRPs) blend the flexibility of polymer materials with the enhanced strength, stiffness, and wear resistance of reinforced materials. These composites are widely used in engineering practices, including the manufacturing of advanced new generation aircraft,[1] wind turbines,[2] *etc.*, replacing the metal counterparts. According to the data, the content of composites in Airbus A350 and Boeing 787 accounts for more than 50% of the total weight.[3,4] CFRPs boast low density, corrosion resistance, and superior mechanical properties, but their low electrical conductivity makes them susceptible to lightning strikes during operating.[5,6] Statistics show that each airplane is struck by lightning more than once yearly or during its 2000–5000 flight hours.[7] Lightning strike is a high-energy, complex, and instantaneous process. The lightning waveform standard comprises multiple strokes of varying intensity and duration with currents ranging from a few hundred amperes to upwards of 200 kA. The transient current rise to 200 kA is conveyed to the CFRP structures in under a few hundred microseconds.[8] The lightning current contributes over 90% of the total energy and will search for an optimal (least resistance) path.[9] The remaining energy converts into light, heat, and shock waves.[10,11] This may cause very substantial damage to the CFRP structure *via* heat, pressure, acoustic shock, and electromagnetic shock.[12–14]

Several engineering compromises have been made to address these issues. For example, aluminum spray coating and expanded metal foils (EMFs) have been generally applied to CFRP surfaces to boost the electrical conductivity in Lightning Strike Protection (LSP) systems used in current aircraft.[15,16] However, critical issues with these metallic materials include high density, poor compatibility, inconsistent coefficients of thermal expansion, and failure under high temperatures.[17] Consequently, advances in conductive materials and structural design technologies have led to the investigation of novel lightning strike protection technologies.[18–22] Low-dimensional, advanced carbon materials, like carbon nanotubes (CNTs) exhibit high electrical conductivity,[13,23] are considered the ideal alternatives for shielding CFRP from lightning strikes. Zhang *et al.* integrated 12-layer CNT thin films into CFRP laminates, which significantly enhanced both in-plane and through-thickness conductivity. Additionally, this modification

[a]*CAS Key Laboratory of Nanosystem and Hierarchical Fabrication, CAS Center for Excellence in Nanoscience, National Center for Nanoscience and Technology, Beijing, 100190, China. E-mail: baiyunxiang0101@163.com; zhangh@nanoctr.cn*

[b]*University of Chinese Academy of Sciences, Beijing, 100049, China*

[c]*CAS Key Laboratory Mechanical Behavior and Design of Materials, Department of Modern Mechanics, University of Science and Technology of China, Hefei, 230027, China. E-mail: zhongzhang@ustc.edu.cn*

[d]*State Key Laboratory of Metastable Materials Science and Technology, College of Materials Science and Engineering, Yanshan University, Qinhuangdao 066004, China*

[e]*CAS Key Laboratory of Standardization and Measurement for Nanotechnology, CAS Center for Excellence in Nanoscience, National Center for Nanoscience and Technology, 100190, Beijing, China*

† Electronic supplementary information (ESI) available. See DOI: https://doi.org/10.1039/d4na00392f

‡ These authors contributed equally to this work.

reduced the damage depth by 68.0% after a 100 kA lightning strike.[24] However, this method does not fully exploit the mechanical advantages of epoxy composites, is not compatible with conventional technology, and is not easy to repair.[20] To address this problem, researchers have preferred applying a highly conductive film directly to the surface of the CFRP laminate. CNT films have low density, high thermostability, good chemical/environmental stability and compatibility with CFRP.[13,23–29] Recently, Han *et al.* used 70 μm thick buckypaper to effectively withstand 40 kA lightning strikes.[27] However, the areal density was still very high.

Glass fibers are typically introduced as an isolation layer between the CFRP and LSP layer.[17] In the laboratory, we set up the Miniature Tip Discharge System (MTDS) and studied the failure mechanisms of the composite system.[30] The results indicated that the isolation layers significantly enhance LSP effectiveness through their thermal resistance and insulation properties. In addition, compared with the metal mesh/foil LSP layer, SA-CNTFs have advantages such as low density, high thermostability, good chemical/environmental stability and compatibility with CFRP, while compared with buckypaper (electrical conductivity < 6000 S m^{-1}), SA-CNTFs have higher purity, higher densification degree, and much better electrical conductivity (~6 × 10^4 S m^{-1}). As a result, we then crafted an advanced composite laminate using quartz fibers for the isolation layers. This laminate, consisting of 1500 SA-CNTF layers and 2 quartz fiber prepreg layers, demonstrated the capacity to withstand a 100 kA lightning strike.[31] Compared to LSP laminates using glass fiber isolation layers, the areal density can be reduced by ~38%. However, both have much room for improvement in thermal resistance and insulating properties compared to lightweight, high-performance ceramic fibers, like zirconia fibers.[32]

In this work, advanced lightweight LSP composites are fabricated using zirconia fiber as the isolation layer. Simulated lightning strikes were employed to explore the LSP performance of the zirconia fiber-based isolation layer and validate the protection mechanism. After lightning strikes, the internal damage level of the composite laminate was assessed using a microfocus X-ray system and non-destructive ultrasonic techniques, and compression tests provided additional evaluation of the damage level. The composite laminate, composed of SA-CNTFs (1000-layer) and zirconia fiber (1-layer), was demonstrated to have the capacity to withstand 100 kA lightning strikes. Furthermore, a weight reduction of ~44.3% and ~10.4% was realized compared to isolation layers composed of glass fiber and quartz fiber, respectively.

Results and discussion

Characterization of the composite laminates

SEM analysis was conducted to characterize the microscopic morphology of composite laminates. Fig. S1a and b† reveal that the zirconia fiber paper consists of a multitude of randomly fibrous networks with a diameter of approximately 4–6 μm. Zirconia fibers are composed solely of the elements oxygen and zirconium, without any doping from additional elements (Fig. S1c†). The zirconia fiber paper was regarded as "isolation layers", and SA-CNTFs were used as "conductive layers" and then embedded with the CFRP laminates by hot compression. The structure of composite laminates is schematically depicted in Fig. 1, and the typical microscopic morphologies of the carbon fiber, zirconia fiber paper, and SA-CNTFs are illustrated in Fig. 1b–d, respectively. The three components (SA-CNTFs, zirconia fiber, CFRP prepreg) of the composite are effectively bonded by epoxy resin. Due to the spaces between the CNTs in the SA-CNTFs and the loose structure of the zirconia fibers, the epoxy resin fully permeates these materials. There are no apparent bubbles between the layers and no resin-rich layer. Moreover, the SA-CNTFs remain super-aligned and have excellent electrical conductivity after curing.

Damage analysis of samples following LS tests

Lightning strike tests were performed with a D waveform to directly assess the LSP properties of composite laminates. To the best of our knowledge, carbon fiber will be severely broken inside the laminate when no conductive layer is on the CFRP surface. The leading causes of severe damage are shockwaves and Joule-heating induced by lightning strikes. Without the addition of SA-CNTFs, the LSP laminate samples remain insulated. Therefore, we do not design a test without a conductive layer.[13,33] However, as the number of layers increases, the electrical conductivity improves significantly. When 1000 layers of CNT film are added, the sheet resistance decreases to 2.56 Ω $\square^{-1}$ (Table S1†). Fig. 2a1 and b1 show that the composite laminate comprises 1000/1200 layer SA-CNTFs and one layer of zirconia fiber paper. The C-scan and B-scan images indicate that

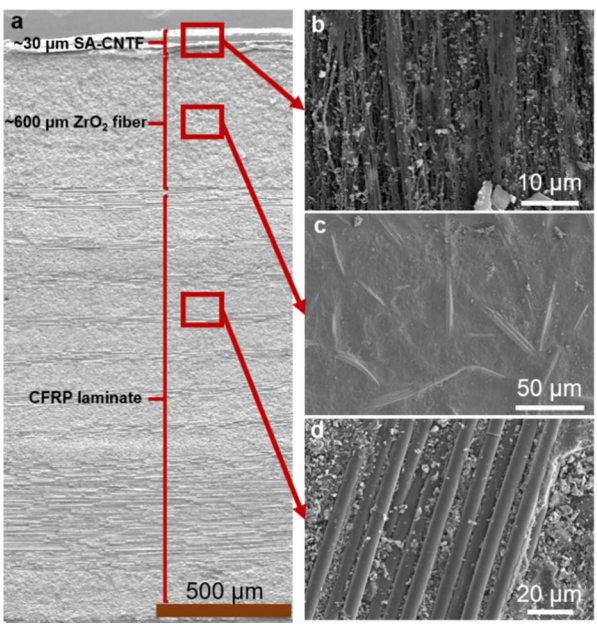

Fig. 1 Typical morphology of the composite laminate. (a) Optical microscopy image of the cross-section of composite laminates, (b)–(d) are the SEM images of the red rectangular area in (d), corresponding to the conductive layer, isolation layer, and CFRP laminate, respectively.

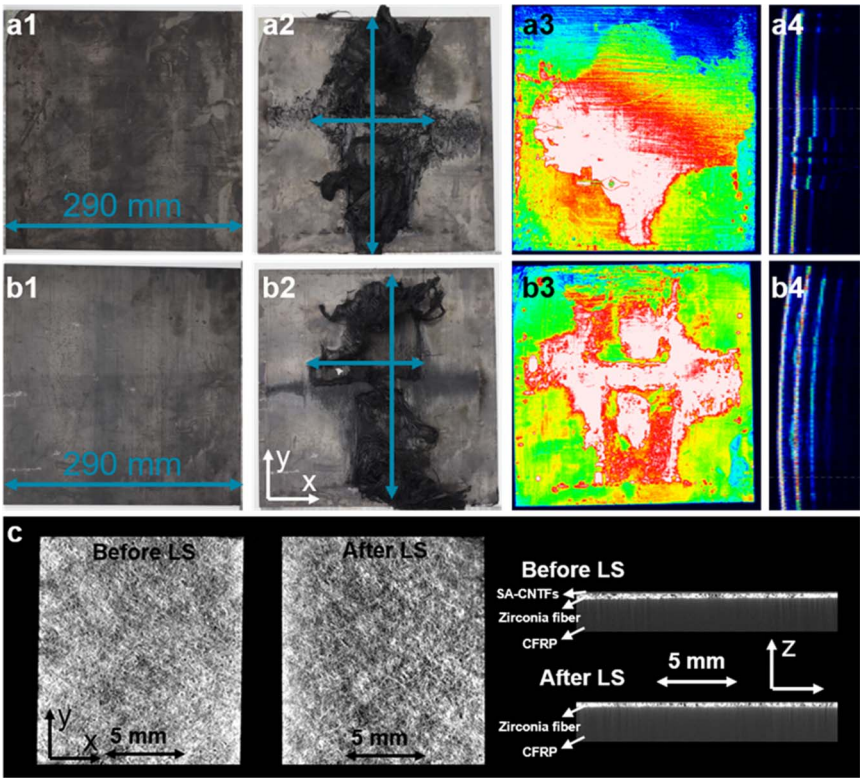

Fig. 2 Damage assessment of composite laminates. (a) Z1C1000. (b) Z1C1200. Images labeled with subscripts 1, 2, 3, and 4 are the digital photographs of composite laminates before LS, after LS, C-scan image, and B-scan image. (c) X-ray image of internal damage to Z1C1200 prior to and following the LS.

the composite laminate surface is flat and free of defects, cracks, and delamination before the lightning strike tests (Fig. S2†). Although the existence of the conductive SA-CNTFs prevents the composite laminates from severe damage, damage to the surface is inevitable after the lightning strike. As shown in Fig. 2a2 and b2, the SA-CNTFs on the composite laminate's surface were severely damaged and debonded from the bottom CFRP laminate after the lightning strike. The damage of SA-CNTFs is observed along the radial direction of CNTs in the middle of the specimen.

The assessment of the effectiveness of LSP involves inspecting the internal damage within composite laminates. Ultrasonic testing provides a non-destructive method for the assessment of the internal damage. The C-scan image and B-scan reveal extensive damage on the surface of the SA-CNTFs along the CNT radial in Z1C1000, while no internal damage is observed within the CFRP laminate (Fig. 2a3 and b3). The specimen exhibits a maximum damaged area of approximately 3.94×10^4 mm^2 and reaches a depth of around 0.3 mm (Table 1). As the number of CNT layers increases to 1200, the damage is reduced, and the B-scan demonstrates a uniform pattern in the cross-section, verifying that the CFRP laminate remains intact (Fig. 2a4 and b4). Furthermore, the specimen exhibits a maximum damage area of approximately 3.75×10^4 mm^2 and a depth of 0.1 mm (Table 1). Significantly, the damage depth of Z1C1200 is lower than that of Z1C1000. The primary reason for this reduction is that an increase in the conductive layer aids in transferring lightning current to the ground, effectively dissipating energy and shielding the laminate from damage. Previous results show that carbon fiber breakage was observed in the composite laminate (damage depth $\sim$ 1.8 mm) composed of 1200-layer SA-CNTFs and 2-layer quartz fiber when suffering the lightning strike with a peak current I_{peak} = 100 kA.[31] Therefore, zirconia fiber demonstrates superior LSP effectiveness compared with quartz fiber. Additionally, a comparison of LSP effectiveness and corresponding surface areal densities with CNT films as conductive layers and different isolation layers is provided in Table 1. Among the materials achieving LSP, zirconia fibers as isolation layers exhibited the lowest areal density. Although the surface damage to these SA-CNTF-based protective materials is very severe, the severely damaged surfaces effectively dissipate the lightning energy, reducing the depth of damage in the thickness direction.

A microfocus X-ray system was utilized to further investigate internal damage in Z1C1200.[13,34] Typical X-ray images of CFRP have a homogeneous light grey signal, suggesting that it is free of cracks and defects. In contrast, if cracks or defects exist, black areas will occur in X-ray images. The size of the black area determines the damage level.[34] Before lightning strikes, the cross-section of composite laminates is divided into three layers: the SA-CNTFs and CFRP are light grey, and the isolation layer is off-white with some black spots. The most severely damaged area of the specimen was selected for the test after lightning strikes. As shown in the vertical cross-section, the morphology of the

Table 1 The sample composition and the damage condition after simulated lightning strikes compared with other composite laminates[a]

		Composition of composite laminates				Extent of damage			
No.	Name	Materials of isolation layers	Layer count of isolation layers	Thickness of CNT films (μm)	Total areal density of isolation layers and conductive layers (g m^{-2})	Damage location	Depth (mm)	Area (mm^2)	Whether protection is achieved or not
1	Z1C1000	ZrO_2 fiber	1	30	206	Surface	~0.3	~3.94 × 10^4	✓
2	Z1C1200	ZrO_2 fiber	1	36	212	Surface	~0.1	~3.75 × 10^4	✓
(Ref. 31) 3	Q3C500	Quartz fiber	3	15	310	Surface	~0.1	~2.82 × 10^4	✓
(Ref. 31) 4	G3C500	Glass fiber	3	15	370	Inside	~2.0	~1.68 × 10^4	✗
(Ref. 31) 5	Q2C1200	Quartz fiber	2	36	224	Inside	~1.8	~2.55 × 10^4	✗
(Ref. 31) 6	Q2C1500	Quartz fiber	2	45	230	Surface	~0.2	~4.07 × 10^4	✓
(Ref. 27) 7	P-IEP-BP-4	Boron nitride	1	70	325	Surface	~0	~860	✓

[a] The "Name" column in the table is defined as follows: Z: zirconia fiber paper. G: glass fiber prepreg. Q: quartz fiber prepreg. C: SA-CNTFs. The numbers indicate the layer count. The labels "Surface" and "Inside" refer to the location of the damaged area, either on the surface or inside. "Depth" represents the maximum depth of the damaged area, while "Area" refers to the largest area of the damaged surface.

isolation layer and CFRP of the specimen after lightning strikes remained consistent with the original specimen, indicating an excellent LSP effect. The disappearance of the light grey color on the surface clearly indicates the absence or break of SA-CNTFs in the top layer, corroborating the SEM results (Fig. 2c).

Possible mechanism of SA-CNTFs and zirconia fiber for LSP

The morphologies of the damaged surface are examined using SEM. As shown in Fig. 3a, the surface SA-CNTFs near the arc attachment point are severely damaged with the aligned CNT network disrupted and extensive resin ablation observed (Fig. 3b and c). To study the LSP mechanism, Raman spectroscopy was conducted. The observed decrease in the I_G/I_D ratio indicated an increase in the prevalence of defects (Fig. 3d). XRD further revealed the phase transitions of the SA-CNTFs during the LS tests. The position of the peak (D_{002}) upshifts slightly, indicating a slight decrease in the interlayer spacing of the CNTs (Fig. 3e). The XPS survey detected variations in the elemental composition of SA-CNTFs prior to and following the LS tests. There was a significant increase in the nitrogen and oxygen elements, indicating the nitrogenization and oxidation of CNTs due to the lightning strike process. As a result, when LS occurs, the conductivity layer channels a portion of the current away. The instantaneous Joule heating from lightning current triggers various chemical reactions and physical processes, including oxidation, nitrogenization, phase change of CNTs, and ablation of resin. Those reactions help to dissipate a portion of the generated heat.[35] However, such small amounts of SA-CNTFs and resin cannot dissipate all the heat alone,[36] and the residual temperature is then conveyed to the underlying layers. An excellent LSP effect can be achieved if the isolation layer effectively dissipates the residual temperature, preventing the temperature transferred to the CFRP from reaching its decomposition temperature.[37]

Consistent with our previous validation results, there are two critical factors: thermal resistance and thermal insulation.[30,31] We tested the thermal insulation performance of different isolation layers to further elucidate the LSP effectiveness of zirconia fiber. Composite laminates consisting of different isolation layers and the same number of layers of carbon fiber prepreg were constructed, and their thermal conductivity in the thickness direction was tested.[38] As listed in Tables 2 and S1,† the thermal conductivity of composite laminates composed of zirconia fiber with CFRP shows the lowest thermal conductivity, followed by glass fiber and quartz fiber. It is widely recognized that the thermal conductivity of surface SA-CNTFs, both axially and radially, spans from tens to hundreds of W m^{-1} K^{-1}, substantially exceeding that of the isolation layer by hundreds of times. Consequently, heat diffusion occurs more efficiently from the SA-CNTFs. Due to the low thermal conductivity of zirconia fibers, the majority of the heat dissipates within the surface layer of the isolation layer and SA-CNTF layer, with only a minimal amount transferring to the CFRP, insufficient to cause damage. Another critical factor is thermal resistance. Zirconia fiber has superior thermal resistance (~2700 °C), much

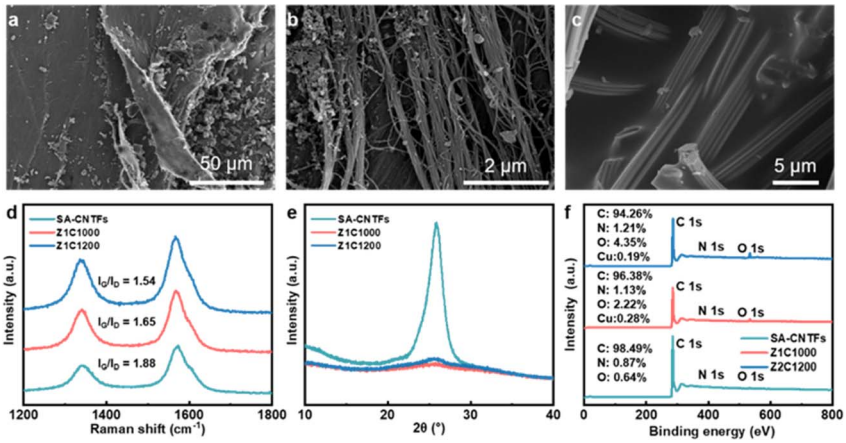

Fig. 3 Characterization of the specimen. (a–c) SEM images of the fracture surface of the specimen after LS tests. (d) Raman spectra of SA-CNTFs prior to and following the LS tests. (e) XRD study of SA-CNTFs prior to and following the LS tests. (f) XPS survey scans of the SA-CNTFs prior to and following the LS tests.

higher than that of quartz fiber (~1700 °C). No melting was observed after the lightning strike, and the zirconia fibers retained their intact shape (Fig. 3c). Therefore, owing to their superior thermal resistance and insulation properties, zirconia fibers are more effective as isolation layer materials than glass and quartz fibers.

Residual strength of the samples following the LS tests

It must be noted that the conductivity layer and isolation layer in composite laminates act as sacrificial layers. Even if the sacrificial layers are damaged or sacrificed, protection is achieved as long as the mechanical properties of the bottom material are maintained.[7,39] The damage level and actual effectiveness against lightning strikes can be visualized in the residual mechanical properties.[40] Lightning strikes can severely damage composite laminates by shock and joule heating induced by lightning currents. Samples in the lightning strike zone are exposed to thermal degradation, and the most severely damaged areas show the worst mechanical properties. The most severely damaged area was selected for the test for the post-strike samples.[17,40] All the laminates were cut into boards measuring 75.0 mm in length and 12.5 mm in width, in compliance with GB/T 3356-2014. The boards were positioned on two supports with a span of 48 mm, with the non-struck side facing upwards to undergo flexural failure. Fig. 4a shows that the load–displacement curves of post-strike Z1C1000 and post-strike Z1C1200 are highly consistent with the pristine samples' curves, indicating that the mechanical properties remain intact after LS. After LS, the residual strengths of Z1C1000 and Z1C1200 are 1222 ± 59 MPa and 1118 ± 50 MPa, respectively,

Table 2 The thermal resistance and thermal conductivity of zirconia fibers compared with other isolation layers used in LSP

Materials	Thermal resistance of isolation layers (°C)	Thermal conductivity of isolation layers with CFRP (W m^{-1} K^{-1})
Zirconia fiber	~2700	0.68
Glass fiber	~900	0.71
Quartz fiber	~1700	0.78

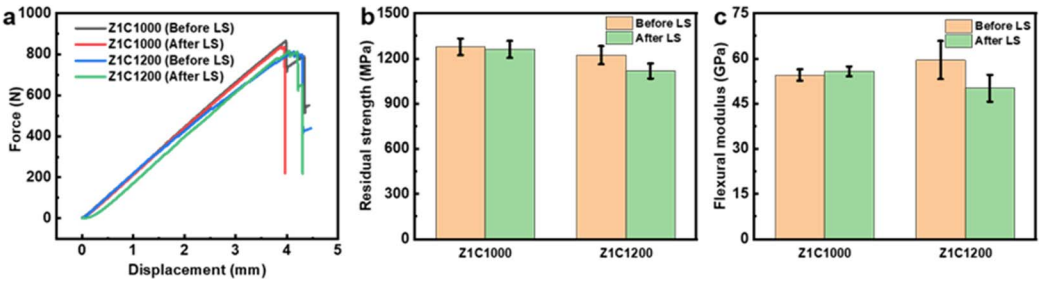

Fig. 4 Residual strength and flexural modulus of the composite laminate after LS tests. (a) Specimens load–displacement curves before and after LS tests. (b) Residual strength of the samples before and after LS tests. (c) Flexural modulus of the samples before and after LS tests.

and the flexural moduli of Z1C1000 and Z1C1200 are 54.55 ± 1.62 GPa and 50.13 ± 4.48 GPa, respectively. The results demonstrate that Z1C1000 could retain residual strengths of more than 98.0% and more than 99.0% of its residual strengths (Fig. 4a and b). For Z1C1200, the residual strengths and modulus remained at 91.4% and 84.0%, respectively. If more than 80% of the composite's residual strength is retained after LS, the composite can be appropriately maintained and reused in engineering applications.[41] In conclusion, the Z1C1000 and Z1C1200 laminates combine lower surface density with excellent LSP performance, making them suitable for continued use in practical applications (Fig. 4).

Conclusions

In this study, we developed a lightweight, advanced LSP system composed of conductive SA-CNTFs and zirconia fibers and further explored its reliability and mechanism for LSP. The conductive SA-CNTFs can provide effective LSP by performing two key functions: conducting current away and aiding in the dissipation of heat generated by lightning currents through processes such as gasification, oxidation, phase change, *etc.* Furthermore, with the lower thermal conductivity and high thermal resistance, the zirconia fibers isolation layer can effectively impede Joule heat transfer to CFRP and provide a good LSP effect. The composite laminate composed of 1000 layers of SA-CNTFs and 1 layer of zirconia fiber paper can shield the CFRP from 100 kA lightning strikes. The excellent LSP effect was demonstrated by the microfocus X-ray system and non-destructive ultrasonic techniques. Consequently, zirconia fibers outperform glass and quartz fibers as isolation materials due to their superior thermal resistance and insulation capabilities, leading to weight reductions of ~44.3% and ~10.4%, respectively.

Experimental section

Materials

SA-CNTFs (1000-layer) with an areal density and thickness of ~20 g m^{-2} and 30 μm, respectively, were supplied by the Department of Physics & Tsinghua-Foxconn Nanotechnology Research Center, Tsinghua University. The higher the number of layers, the higher the surface density and thickness (for a more detailed preparation process, please see Text S1†).[29] Epoxy adhesive films with an areal density of ~90 g m^{-2} were used. Unidirectional carbon fiber prepregs (G125000) with a thickness of 0.1 mm were purchased from Shanghai HuanXu Group Co., Ltd. The areal density was ~100 g m^{-2}, with a fiber weight fraction of 60%. ZrO_2 fiber paper with an areal density of ~96 g m^{-2} and a thickness of 0.6 mm was purchased from Foshan Inai Energy Saving Material Co., Ltd.

Preparation of composite laminates

The method for preparing composite laminates follows the curing procedure recommended in our previous study.[31] Carbon fiber prepreg, zirconia fiber paper, and SA-CNTFs were sequentially layered and subsequently hot-pressed to obtain composite laminates. Composite laminate compositions are provided in Table 1.

Lightning strike test

The simulated lightning strike test is conducted at the Hefei Hangtai Electrophysics Co., Ltd. The lightning strike tests are guided by the SAE ARP 5416A-2013 standard lightning strike introduction test.[8] For this research, the D waveform (I_{peak} = 100 kA) was simulated on the composite laminates. The laminate was clamped and electrically grounded by a copper plate. And the discharged electrode was located at the center of the laminate and linked with a copper wire.

Other characterization

The severity of damage was inspected with non-destructive ultrasonic testing. The B-scan and C-scan images obtained by non-destructive ultrasonic testing can be analyzed to determine the damage depth and area of composite laminates.[42,43] (For further details on how to analyze this, please refer to our earlier publication.)[31] A microfocus X-ray system (Xradia 520 Versa, Zeiss) was used to further evaluate the internal damage of composite laminates. The scanning voltage was set at 60 kV (83 μA), with an exposure time of 3 seconds for each radiograph. The Scout-and-Scan Control System Reconstructor software was utilized for reconstructing each scan volume, with manipulation and analysis conducted using XM3D Viewer software. The surface morphologies of composite laminates were characterized by scanning electron microscopy (Hitachi SU8220). The elemental composition was analyzed by energy-dispersive X-ray spectroscopy mapping (SEM-EDS). X-ray photoelectron spectroscopy was used to analyze the elemental content of SA-CNTFs. Raman spectra for the SA-CNTFs were acquired using a Renishaw inVia Plus Raman spectrometer, equipped with a 514 nm laser. The overhead view of laminates was obtained by a digital camera (Canon, ESO M50). The compressive strengths of composite laminates were measured using an MTS C45 105 Universal Testing Machine under the GB/T 3356-2014 standard. Additionally, the "laser flash" technique (LFA467, Netzsch) along with differential scanning calorimetry (DSC, Q2000) was employed to evaluate the through-thickness thermal diffusivity (α) and heat capacity (C_p), respectively. Subsequently, the thermal conductivity (K) was subsequently calculated using the equation $K = \alpha\rho C_p$, where ρ represents the density of composite laminates.

Data availability

The data supporting this article have been included as part of the ESI.†

Author contributions

Conceptualization: ZZ, HZ, YB, MZ. Methodology: MZ, FG, YB, MZ. Investigation: ZZ, HZ, YB, MZ. Visualization: MZ, FG, FG. Funding acquisition: ZZ. Project administration: ZZ, HZ, YB.

Supervision: ZZ, HZ, YB. Writing – original draft: MZ, PZ, FG, YB. Writing – review & editing: ZZ, LL, HZ, YB, MZ, PZ, FG.

Conflicts of interest

The authors declare no competing financial interest in this work.

Acknowledgements

This work was supported by the National Key Basic Research Program of China (grant no. 2022YFA1205400).

Notes and references

1 B. Parveez, M. I. Kittur, I. A. Badruddin, S. Kamangar, M. Hussien and M. A. Umarfarooq, *Polymers*, 2022, **14**, 5007.
2 P. Veers, K. Dykes, E. Lantz, S. Barth, C. L. Bottasso, O. Carlson, A. Clifton, J. Green, P. Green and H. Holttinen, *Science*, 2019, **366**, eaau2027.
3 K. Lu, *Science*, 2010, **328**, 319–320.
4 Q. Dong, Y. Guo, X. Sun and Y. Jia, *Polymer*, 2015, **56**, 385–394.
5 H. Kawakami, *Lightning Strike Induced Damage Mechanisms of Carbon Fiber Composites*, University of Washington, 2011.
6 Y. Guo, Y. Xu, Q. Wang, Q. Dong, X. Yi and Y. Jia, *Compos. Sci. Technol.*, 2019, **169**, 95–102.
7 V. Kumar, T. Yokozeki, C. Karch, A. A. Hassen, C. J. Hershey, S. Kim, J. M. Lindahl, A. Barnes, Y. K. Bandari and V. Kunc, *Composites, Part B*, 2020, **183**, 107688.
8 A.-L. Committee, *Aircraft Lightning Test Method ARP5416*, SAE International, 2013.
9 V. Mazur, *Principles of Lightning Physics*, IOP Publishing, 2016.
10 V. Kumar, T. Yokozeki, C. Karch, A. A. Hassen, C. J. Hershey, S. Kim, J. M. Lindahl, A. Barnes, Y. K. Bandari and V. Kunc, *Composites, Part B*, 2020, **183**, 107688.
11 J. Lee, T. E. Lacy, C. U. Pittman and J. N. Reddy, *Compos. Struct.*, 2019, **224**, 111039.
12 P. Feraboli and M. Miller, *Composites, Part A*, 2009, **40**, 954–967.
13 B. Wang, Y. Duan, Z. Xin, X. Yao, D. Abliz and G. Ziegmann, *Compos. Sci. Technol.*, 2018, **158**, 51–60.
14 X. Zhang, X. Tian, N. Wu, S. Zhao, Y. Qin, F. Pan, S. Yue, X. Ma, J. Qiao, W. Xu, W. Liu, J. Liu, M. Zhao, K. Ostrikov and Z. Zeng, *Sci. Adv.*, 2024, **10**(11), eadl6498.
15 M. Gagné and D. Therriault, *Prog. Aerosp. Sci.*, 2014, **64**, 1–16.
16 Y. Guo, Y. Xu, Q. Wang, Q. Dong, X. Yi and Y. Jia, *Composites, Part A*, 2019, **117**, 211–218.
17 Y. Guo, Y. Xu, L. Zhang, X. Wei, Q. Dong, X. Yi and Y. Jia, *Compos. Sci. Technol.*, 2019, **174**, 117–124.
18 P. S. M. Rajesh, F. Sirois and D. Therriault, *Mater. Des.*, 2018, **139**, 45–55.
19 S. Yamashita, Y. Hirano, T. Sonehara, J. Takahashi, K. Kawabe and T. Murakami, *Composites, Part A*, 2017, **101**, 185–194.
20 Z. J. Zhao, G. J. Xian, J. G. Yu, J. Wang, J. F. Tong, J. H. Wei, C. C. Wang, P. Moreira and X. S. Yi, *Compos. Sci. Technol.*, 2018, **167**, 555–562.
21 J. Gou, Y. Tang, F. Liang, Z. Zhao, D. Firsich and J. Fielding, *Composites, Part B*, 2010, **41**, 192–198.
22 J. Langot, E. Gourcerol, A. Serbescu, D. Brassard, K. Chizari, M. Lapalme, A. Desautels, F. Sirois and D. Therriault, *Composites, Part A*, 2023, **175**, 107772.
23 V. Kumar, S. Sharma, A. Pathak, B. P. Singh, S. R. Dhakate, T. Yokozeki, T. Okada and T. Ogasawara, *Compos. Struct.*, 2019, **210**, 581–589.
24 J. Zhang, X. Zhang, X. Cheng, Y. Hei, L. Xing and Z. Li, *Composites, Part B*, 2019, **168**, 342–352.
25 D. K. Chakravarthi, V. N. Khabashesku, R. Vaidyanathan, J. Blaine, S. Yarlagadda, D. Roseman, Q. Zeng and E. V. Barrera, *Adv. Funct. Mater.*, 2011, **21**, 2527–2533.
26 J. S. Bulmer, A. Kaniyoor and J. A. Elliott, *Adv. Mater.*, 2021, **33**, e2008432.
27 J.-h. Han, H. Zhang, M.-j. Chen, D. Wang, Q. Liu, Q.-l. Wu and Z. Zhang, *Carbon*, 2015, **94**, 101–113.
28 Q. Xia, H. Mei, Z. Zhang, Y. Liu, Y. Liu and J. Leng, *Composites, Part B*, 2020, **180**, 107563.
29 Y. Bai, M. Zhu, S. Wang, L. Liu and Z. Zhang, *Carbon*, 2023, **202**, 425–431.
30 Y. Bai, M. Zhu, S. Wang, F. Gao, R. Gao, Y. Qu, X. Cui, G. Wang, L. Liu, H. Zhang and Z. Zhang, *Composites, Part A*, 2023, **167**, 107394.
31 Y. Bai, M. Zhu, S. Wang, F. Gao, R. Gao, C. Wang, G. Wang, H. Jin, L. Liu, H. Zhang and Z. Zhang, *Composites, Part A*, 2023, **173**, 107617.
32 B. Li, H. Tian, L. Li, W. Liu, J. Liu, Z. Zeng and N. Wu, *Adv. Funct. Mater.*, 2024, 2314653.
33 H. Zhu, K. Fu, B. Yang and Y. Li, *Compos. Sci. Technol.*, 2021, **207**, 108675.
34 G. P. McCombe, J. Rouse, R. S. Trask, P. J. Withers and I. P. Bond, *Composites, Part A*, 2012, **43**, 613–620.
35 Q. Xia, H. Mei, Z. Zhang, Y. Liu, Y. Liu and J. Leng, *Composites, Part B*, 2020, **180**, 107563.
36 G. Abdelal and A. Murphy, *Compos. Struct.*, 2014, **109**, 268–278.
37 Y. Guo, Y. Xu, Q. Wang, Q. Dong, X. Yi and Y. Jia, *Compos. Sci. Technol.*, 2019, **169**, 95–102.
38 S. Kamiyama, Y. Hirano, T. Okada and T. Ogasawara, *Compos. Sci. Technol.*, 2018, **161**, 107–114.
39 X. Li, Y. Zhou, S. Kamiyama, T. Okada and T. Yokozeki, *Composites, Part A*, 2024, **177**, 107933.
40 V. Kumar, T. Yokozeki, T. Okada, Y. Hirano, T. Goto, T. Takahashi and T. Ogasawara, *Composites, Part A*, 2018, **114**, 429–438.
41 H. Chu, Q. Xia, Z. Zhang, Y. Liu and J. Leng, *Carbon*, 2019, **143**, 204–214.
42 C. J. Norris, I. P. Bond and R. S. Trask, *Composites, Part A*, 2011, **42**, 639–648.
43 G. J. Williams, I. P. Bond and R. S. Trask, *Composites, Part A*, 2009, **40**, 1399–1406.